#322

ISIS 2

ELECTRON DENSITY + TEMPERATURE

71-024A-07A

ISIS 2

ELECTRON DENSITY + TEMPERATURE

71-024A-07A

THIS DATA SET HAS BEEN RESTORED. THERE WERE ORIGINALLY 8 BINARY 9-TRACK, 1600 BPI TAPES. THERE ARE 3 RESTORED TAPES. THE DR TAPES ARE 3480 CARTRIDGES AND THE DS TAPES ARE 9-TRACK, 6250 BPI. THE TAPES WERE CREATED ON AN IBM 360 COMPUTER. THE DR AND DS NUMBERS ALONG WITH THE CORRESPONDING D NUMBERS AND THE TIME SPAN ARE AS FOLLOWS:

DR#	DS#	D#	FILES	TIME SPAN
DR02976	DS02976	D20541	1	04/14/71 - 05/31/71
		D20542	2	06/01/71 - 09/30/71
		D20543	3	10/01/71 - 12/31/71
DR02977	DS02977	D20544	1	01/01/72 - 02/29/72
		D20545	2	03/01/72 - 05/31/72
		D20546	3	06/01/72 - 10/01/72
DR02978	DS02978	D20547	1	10/01/72 - 12/31/72
		D20548	2	01/01/73 - 03/31/73

REQ. AGENT	RAND NO.	ACQ. AGENT
JVD	RC4288	LLD

ISIS 2

ELECTRON DENSITY + TEMPERATURE

71-024A-07A

This data set consists of 8 tapes that are 9 track, 1600 BPI, Binary, 1 file made on the IBM 360.

The tapes are as follows:

D#	C#	TIME SPAN
D-20541	C-17056	4/14/71 - 5/31/71
D-20542	C-17057	6/01/71 - 9/30/71
D-20543	C-17058	10/01/71 - 12/31/71
D-20544	C-17059	1/01/72 - 2/29/72
D-20545	C-17060	3/01/72 - 5/31/72
D-20546	C-17061	6/01/72 - 10/01/72
D-20547	C-17062	10/01/72 - 12/31/72
D-20548	C-17063	1/01/73 - 3/31/73

ISISB FORMAT

NEW	
A(1)	DAY OF YEAR
A(2)	PASS NO.
A(3)	GEODETIC LAT.
A(4)	GEODETIC LONG.
A(5)	ALT.
A(6)	DATE
A(7)	GMT
A(8)	T(E)
A(9)	N(E)
A(10)	L
A(11)	DIP LAT.
A(12)	SOLAR ZENITH ANGLE
A(13)	CONFIDENCE VALUE FOR T(E)
A(14)	GEOMAGNETIC LAT.
A(15)	GEOMAGNETIC LONG.
A(16)	L. T.
A(17)	DIP
A(18)	SAT. POTENTIAL
A(19)	PROBE 0=BOTTOM 1=TOP
A(20)	INVARIANT LAT.
A(21)	VELOCITY ANGLE
A(22)	MAGNETIC FIELD ANGLE
A(23)	SUN ANGLE
A(24)	MAGNETIC LOCAL TIME

B74885

UNITED STATES GOVERNMENT

Memorandum

TO : Lee Dubach, NSSDC

DATE: December 21, 1972

FROM L. H. Brace, ISIS-I Probe Investigator

SUBJECT Qualification of ISIS-I electrostatic probe measurements

The ISIS-I probe measurements of electron temperature (T_e) and concentration (N_e) that we have submitted to the data center require a certain amount of qualification with regard to their accuracy. In this letter, which can be copied for the use of prospective data users, I will attempt to outline what we know about the accuracy of these measurements.

The goal of the computer analysis program was to evolve an automatic system that reflected an appropriate balance between measurement accuracy on one hand and economy of computer time on the other. The latter is necessary to permit a large fraction of the data to be analyzed given the limited amounts of computer time available for this analysis.

In the process of developing the program we found that the data base had a whole spectrum of data quality. Much of it consisted of nearly ideal volt-ampere curves that could be handled by a relatively simple program. However some of the raw data suffers from such problems as sounder-induced interference, ionospheric fine structure, photoemission from the spacecraft and in cases of very low electron density, positive spacecraft potentials. Since it is often necessary in correlative studies to provide measurements with whatever accuracy is possible, we have had to stretch our criteria for eligible curves rather extensively. As a result, it is sometimes possible for the analysis program to fail to get a value for T_e or N_e, or to get values that are in error. However we have reached a compromise program that can analyze a very large fraction of the data it encounters (> 90%) and will usually provide accuracies within 10% of the value that could be obtained with a more careful hand analysis.

The absolute values for T_e may be high by up to 10% because of experimental factors not easily corrected for and because of a tendency of the exponential fitting routine to fit too far up the curve, especially at temperatures below 2000°k. At higher T_e, more samples are available in the exponential region, and the accuracy improves.

Buy U.S. Savings Bonds Regularly on the Payroll Savings Plan

The N_e values have been correlated with sounder-derived values, using the local plasma frequency, and are found to be systematically high by about 20-30%. This factor varies with satellite attitude and the value of N_e in a manner that has not been fully evaluated. If greater absolute accuracy is needed, I would suggest using the sounder-derived value.

In summary, then, it is important for users to note that all of the measurements are not equally good quality. If the user requires the greatest possible accuracy from a given set of data, it will be necessary to request us to scan the original data set to evalute the accuracy or, alternatively, to reanalyze the data with a program that is more specific to that particular set of data. We will be happy to do that for limited amounts of data.

L H Brace

Larry H. Brace

B15644

Duplicate copy

X-621-73-49

69-009A-07D

AN OVERVIEW OF THE ISIS-I ELECTROSTATIC PROBE MEASUREMENTS OF ELECTRON TEMPERATURE AND CONCENTRATION

L. H. BRACE
R. F. THEIS
J. JOHNSTON

FEBRUARY 1973

GSFC

GODDARD SPACE FLIGHT CENTER
GREENBELT, MARYLAND

X-621-73-49

AN OVERVIEW OF THE ISIS-I ELECTROSTATIC PROBE MEASUREMENTS OF ELECTRON TEMPERATURE AND CONCENTRATION

L. H. Brace
R. F. Theis
J. Johnston

February 1973

GODDARD SPACE FLIGHT CENTER
Greenbelt, Maryland

AN OVERVIEW OF THE ISIS-I ELECTROSTATIC PROBE MEASUREMENTS OF ELECTRON TEMPERATURE AND CONCENTRATION

L. H. Brace
R. F. Theis
J. Johnston

ABSTRACT

The ISIS-I satellite is providing a comprehensive view of many of the parameters of the upper F-region between about 600 and 3500 kilometers. In this report we present a broad overview of the measurements of electron temperature and concentration made by one of the ISIS-I instruments, the cylindrical electrostatic probe. The global structure and its temporal behavior are presented as weekly pole-to-pole plots of the measurements and their locations in altitude and local time. The measurements cover the time interval between January 30, 1969 through June 6, 1971. The high inclination (88.4°) and eccentric nature of the orbit permit both the latitudinal and altitudinal structure of the ionosphere to be resolved during this more than two-year period of decreasing solar activity. As a matter of interest we point out a number of ionospheric features that are being studied for publication elsewhere, including the plasmapause, the effects of precipitation in the region of the high latitude cusp, and the behavior of the ionosphere in the nightside of the auroral zone.

CONTENTS

	Page
ABSTRACT	iii
INTRODUCTION	1
THE METHOD	1
THE GLOBAL PATTERNS OF T_e AND N_e	7
DISCUSSION OF MAJOR FEATURES OF THE DATA	9
Altitudinal Gradients in T_e and N_e	9
The Plasmapause	11
The Cusp Ionosphere	11
A Dynamic View of the ISIS-I Data	11
ACKNOWLEDGEMENTS	12
REFERENCES	13

ILLUSTRATIONS

Figure		Page
1	The ISIS-I spacecraft showing location of the two cylindrical probes	2
2	Configuration of the Sensors	4
3	Simplified Block Diagram of the Electronics	5
4	Computer plot format for the display of raw data (volt-ampere curves) and computer fitting of the curves for N_e and T_e	6
5	Data and Computer Fits for a Low T_e Pass at Low Latitudes at Night and at About 800 Kilometers	8
6	A Typical Week of ISIS-I Probe Measurements Plotted vs Dip Latitude	10

AN OVERVIEW OF THE ISIS-I ELECTROSTATIC PROBE MEASUREMENTS OF ELECTRON TEMPERATURE AND CONCENTRATION

INTRODUCTION

The ISIS-I satellite was launched on January 30, 1969 into a 600 by 3500 kilometer, near-polar orbit ($i = 88.4°$). The satellite and its scientific instruments have been described briefly elsewhere (Florida, 1969) (Whitteker, et al., 1972). The purpose of this report is to provide an overview of the measurements of electron temperature, T_e, and concentration, N_e, made by one of the ISIS-I instruments, the cylindrical electrostatic probe.

During the last solar minimum a similar instrument was employed on Explorer 22 to resolve the global structure and diurnal behavior of the ionosphere at a fixed altitude of about 1000 kilometers (Brace et al., 1967). The ISIS-I satellite measurements now make it possible to investigate the global structure of the ionosphere at solar maximum and beyond. In addition, the eccentricity of the orbit permits altitudinal variations to be derived, although it is not a trivial task to separate the altitude structure from the latitudinal variations. In general this can only be done statistically with the aid of empirical models that are based on a great number of measurements well distributed in latitude and extending over several orbital precession and apsidal rotation periods. The more than two years of probe measurements now available from ISIS-I provides an adequate data base for such a study. Mayr et al. (1972) have reported some initial results of such a model.

THE METHOD

Langmuir probes of the cylindrical type used on ISIS-I have been used extensively on satellites since 1963 when the first ones were flown on Explorer 17 (Brace and Spencer, 1964) (Brace, Spencer, Dalgarno, 1965). The theoretical basis for the method has been described extensively (c.f., Mott-Smith and Langmuir, 1926). The manner in which the method is employed on rockets and satellites has been described by Spencer et al. (1965) and Brace and Reddy (1965), while some of the possible sources of error have been evaluated experimentally by Brace, Findlay and Carignan (1971).

Figure 1 shows the mounting location of the ISIS-I probes. One was mounted on a boom about one meter in length and the other was mounted on the spin axis at the opposite end of the spacecraft. In this arrangement the boom probe provides some volt-ampere curves that are free of the spacecraft wake at least some time within the satellite spin cycle, while the axial probe is capable of unperturbed

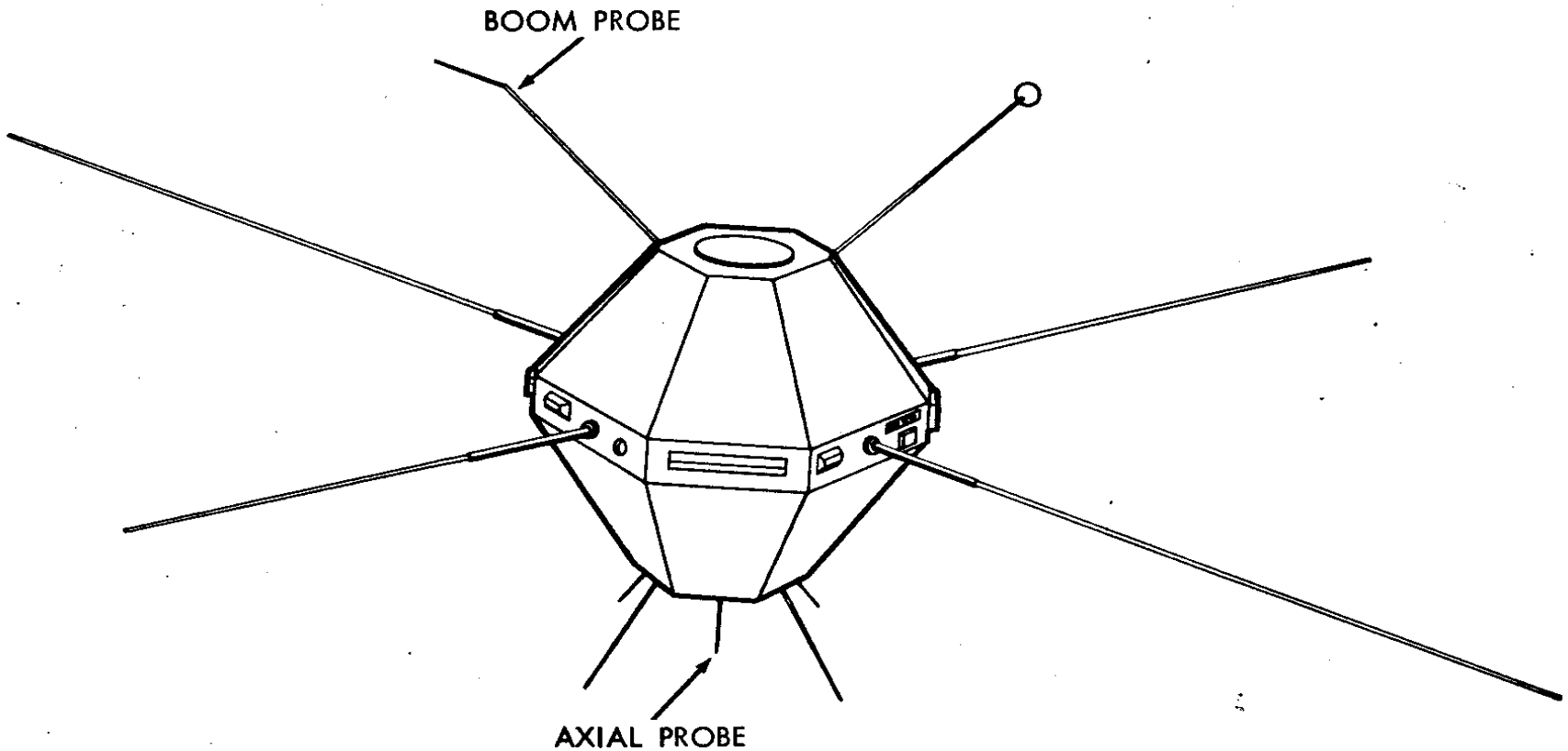

Figure 1. The ISIS-I Spacecraft showing location of the two cylindrical probes. The boom probe is about 1.2 meters away from the spacecraft and perpendicular to the spin axis. The axial probe is mounted on the spin axis at the opposite end of the spacecraft.

measurements only when it preceeds the spacecraft through the plasma. For this reason most of the data presented here are taken from the boom probe, although the axial probe can be used when the added spatial resolution is required.

The sensors consist of three concentric stainless steel tubes that are electrically isolated and arranged as shown in Figure 2. The largest element is the floating guard whose purpose is to place the driven guard and collector well into the plasma, i.e., well away from the disturbed region immediately surrounding the spacecraft. This element floats at its own equilibrium potential. The guard element is 0.165 cm in diameter and acts as an electrical guard for the collector. The collector itself is 0.058 cm in diameter and 23 cm long.

The electronic unit that operates the two probes is shown in simplified block diagram form in Figure 3. It is preprogrammed to operate each probe during alternate two-minute intervals. During each two-minute sequence, four linear electrometer ranges are employed sequentially to resolve the current characteristics of the probe as its voltage is swept from -2 to +10 volts with a period of 2 seconds. The full scale currents are 20, 2, 0.2, 0.02 microamperes, respectively. These ranges permit the curves to be resolved over a density range of about 1×10^2 to 4×10^5/cc. The telemetry system provides 240 analog samples per curve, with eight bit accuracy. Thus current samples are taken at 50 millivolt sweep intervals.

Figure 4 shows the format of the computer plots that are used to display each two-minute segment of the data from a given probe. The top sequence is from the 20 μa range which has little deflection at this time. The lower sequences show the curves on consecutively more sensitive ranges. For a more concise presentation the 15 curves in each range are overlapped in time (horizontally) in this format. Since the satellite spin period is typically 20 seconds, a spin modulation of the curves that may be present can be seen within a given curve sequence. For example, in this case, the spin modulation in the ion current can be seen on the 0.02 μa range. At other spacecraft orientations, spin modulation of the electron current may also be present.

Figure 4 also illustrates the method of data analysis for N_e and T_e. The higher current ranges (2 μa and 0.2 μa in this case) resolve the electron saturation currents that are collected when the probe is driven above the plasma potential and therefore attracts electrons from the plasma. The amplitude of the saturation region is directly proportional to N_e. The more sensitive ranges resolve the electron retarding region whose shape is sensitive to T_e. The solid lines that are superposed on the 0.2 μa curves represent a computer plotted fit of an equation given by Mott-Smith and Langmuir (1926) of the form

$$I_e = AN_e \ (1 + BV)^{1/2} \qquad (1)$$

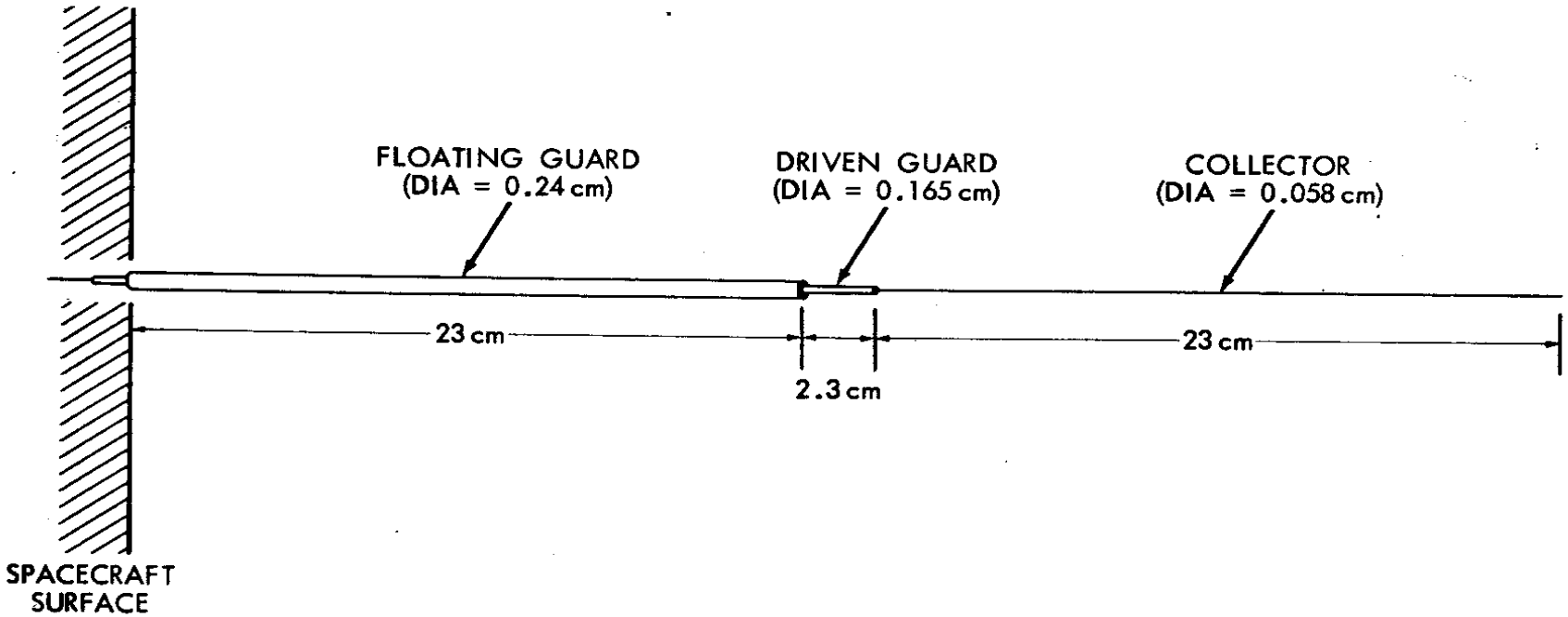

Figure 2. Configuration of the Sensors

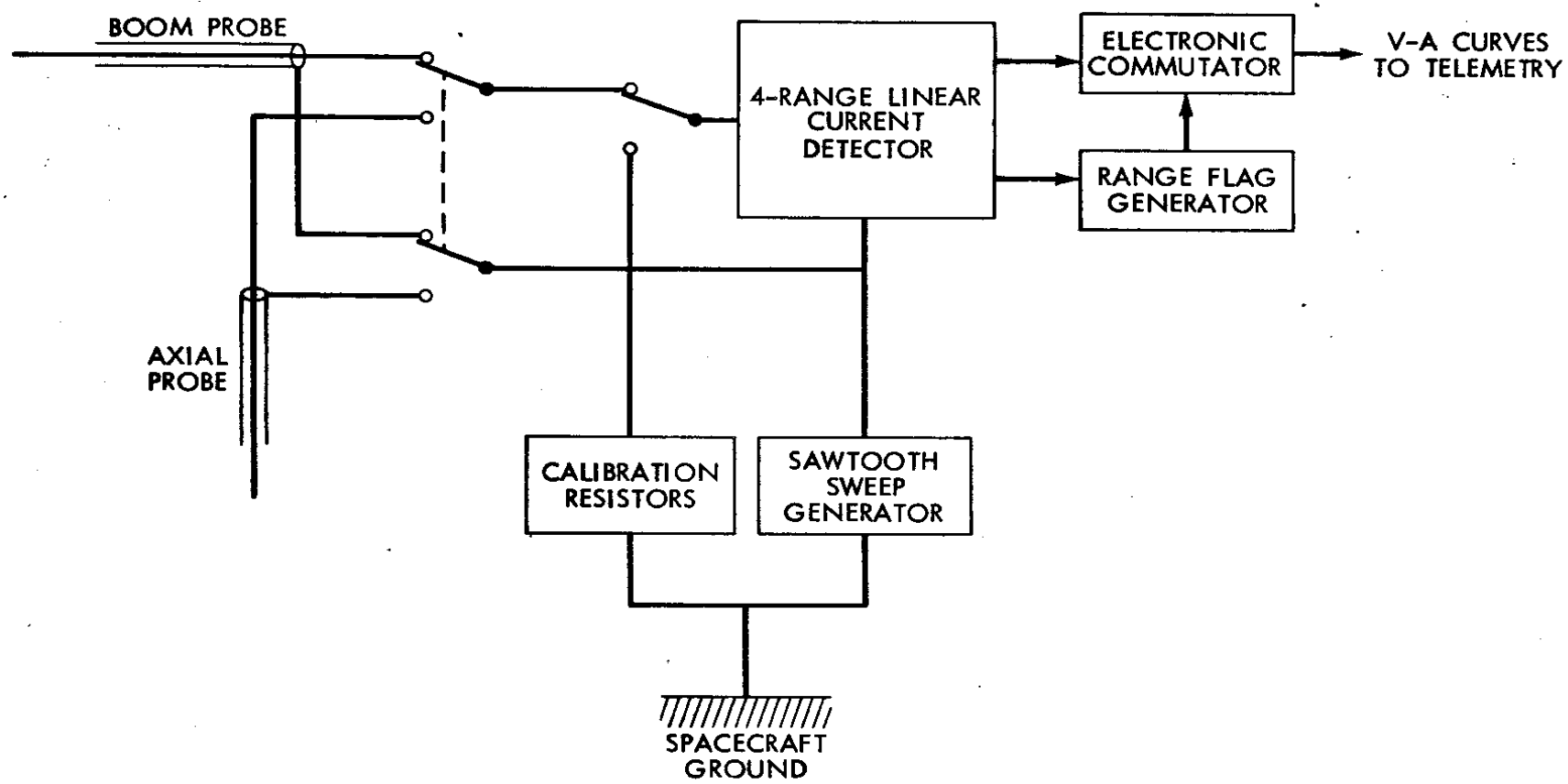

Figure 3. Simplified Block Diagram of the Electronics

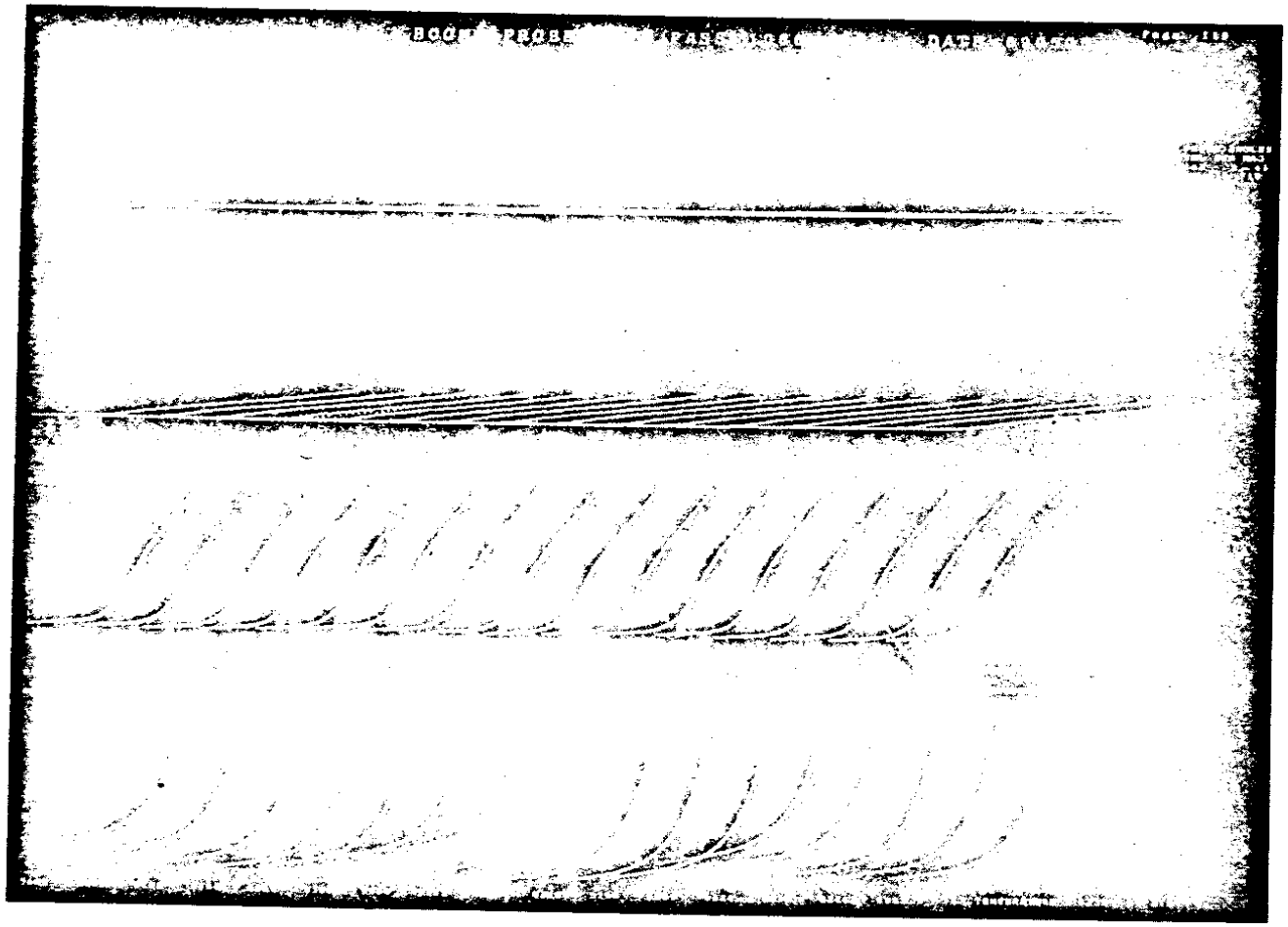

Figure 4. Computer plot format for the display of raw data (volt-ampere curves) and computer fitting of the curves for N_e and T_e. This pass was taken near the equator at 3500 kilometers during midday. The computer fits of the accelerating regions for N_e and the retarding regions for T_e are shown on the 0.2 and 0.02μa ranges, respectively.

where A and B include physical constants and known dimensions of the collector, and V is the probe potential relative to the plasma, a point identified as the inflection point of the curve. The value of N_e that is computed from each curve is listed below the start point of the curve, and an average of the N_e from all curves is listed at the right, suitably weighted by a quality of fit number for each curve.

Similarly the value of T_e is derived by fitting the retarding region with an equation of the form

$$I = A + BV + C \exp (eV/kT_e) \tag{2}$$

where A, B, C and T_e are free parameters of the fit. The solid lines superposed on the 0.02 μa curves represent the fits for T_e. The term A + BV represents an approximation to the ion component of the current, while the electron current component is represented by the exponential term. From the closeness of fit observed on the 0.02 μa range, equation (2) appears to be a rather good representation of the curves. As before, the individual values of T_e are listed below each curve and an average of the entire 30-second interval is listed at the right of the sequence, again suitably weighted by the quality of fit for each curve.

The computer program will attempt to derive a value for N_e and T_e from whichever current ranges show adequate deflection and obey certain obvious criteria for being good curves. For example, fitting of the 0.2 μa curves for T_e was attempted, but these values are not used when better resolution is available on a subsequent range.

Another example of the raw data is shown in Figure 5, where the ionosphere temperature was about 1100°K. Although N_e was higher on this pass our program was unable to fit the 0.2 μa curves for T_e because of the few data points in the exponential region and the inherently lower amplitude of the retarding region at low T_e. However, the most sensitive range (0.02 μa) provided very good fits, except for a series of three or four curves in the middle where sounder interference was most pronounced. Sounder interference is seen also in some of the 20 μa and 2 μa curves and has been a continuing problem in machine analysis of the data.

THE GLOBAL PATTERNS OF T_e AND N_e

The ISIS-I satellite is operated such that data are acquired in the form of 15 to 20 minute intervals at various places about the orbit where the satellite can be

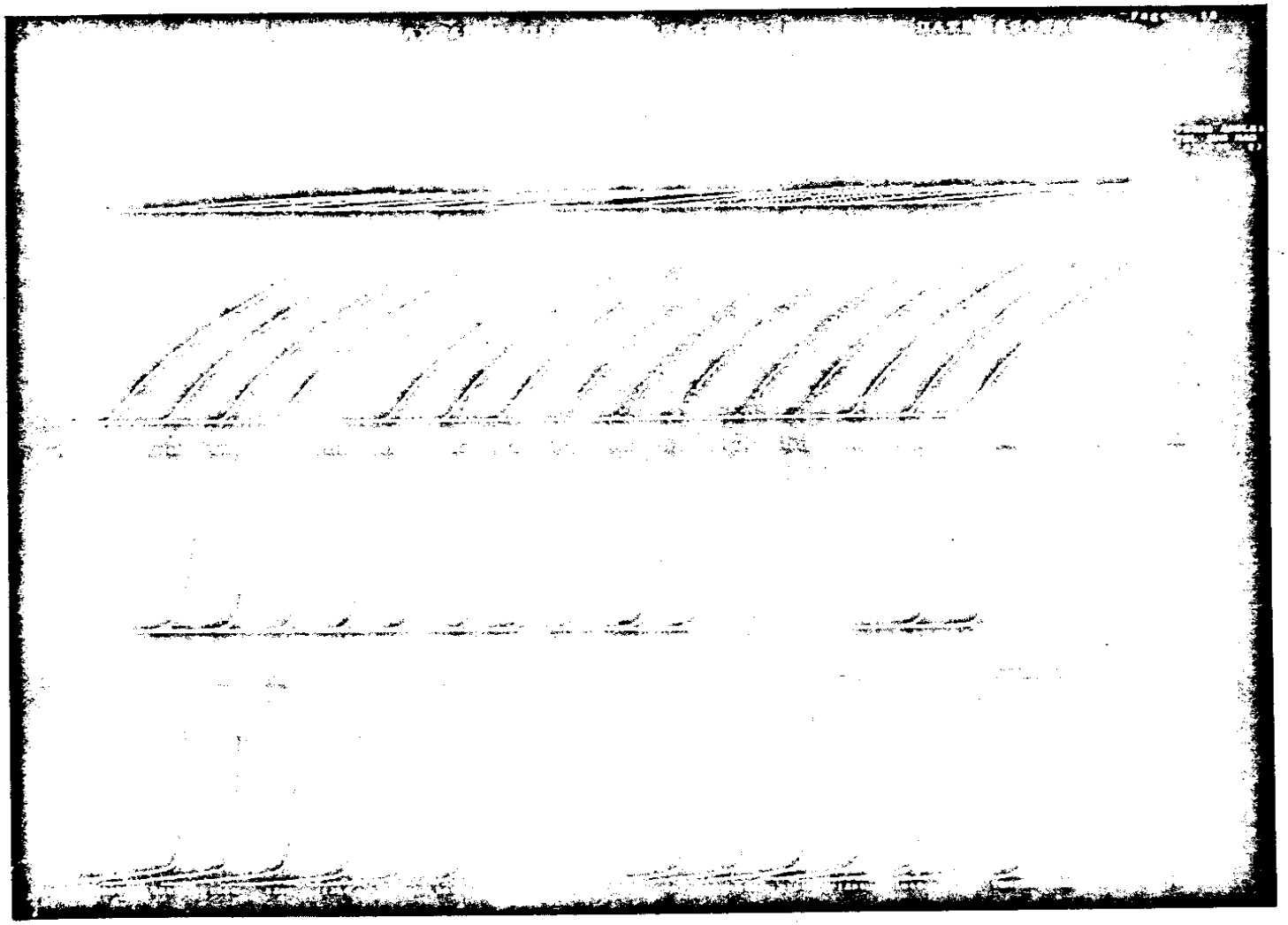

Figure 5. Data and computer fits for a low T_e pass at low latitudes at night and at about 800 kilometers.

interrogated by one of the NASA-STADAN stations or one of the stations operated by countries participating in the ISIS program (Franklin, Bibby, Hitchcock, 1969). An onboard tape recorder provided additional geographic coverage during the first year in orbit. The most extensive latitudinal coverage is obtained at U.S. longitudes, although there is broad longitudinal coverage above 30°N because of the stations at Alaska, England and Norway. However, because of the limited frequency of coverage at low latitudes, complete latitudinal coverage can be obtained only by combining the data from several days of operation. Since the orbital precession rate induces a local time drift of only one hour per week and an apsidal rotation of only 15°, one can obtain a fairly consistent global pattern from a weekly plot of the measurements. Figure 6 shows a typical week of measurements plotted versus magnetic dip latitude. Dip latitude was selected as the abscissa because of the very strong magnetic control that is evidenced by many features of the topside ionosphere. Dip latitude also includes the variation of the real field (based on the dip angle) without introducing discontinuties at the equator such as those experienced when plotting versus L or invariant latitude.

In addition to the values of T_e and N_e, Figure 6 shows the altitude and local times of the measurements. The measurements shown represent the 30-second averages taken every 4 minutes by the boom-mounted probe. Consecutive measurements within a particular pass are connected by solid lines to distinguish the instantaneous structure from the variations that occur from one pass to another. The latter variations reflect both real changes with UT as well as longitudinal structure in the ionosphere.

The remaining figures in this report simply show the weekly plots of T_e and N_e for the period from 30 January 1969 to 5 June 1971. These represent the data analyzed to date. We make no attempt in this report to interpret these data but simply present them as an attempt to convey a feeling for the nature of the data base that is now available for analysis. A number of studies using these data have been published, or submitted, and others are being prepared.

DISCUSSION OF MAJOR FEATURES OF THE DATA

Although we leave any detailed interpretation of the data to other reports, a number of ionospheric features and properties are so clearly evident in these global plots that they should be briefly noted.

Altitudinal Gradients in T_e and N_e

As noted earlier, it is often difficult from a single plot such as Figure 6 to distinguish between altitudinal and latitudinal structure. However, during those weeks when perigee is nearly on the equator (week of 69 10 20 - 10 25), the

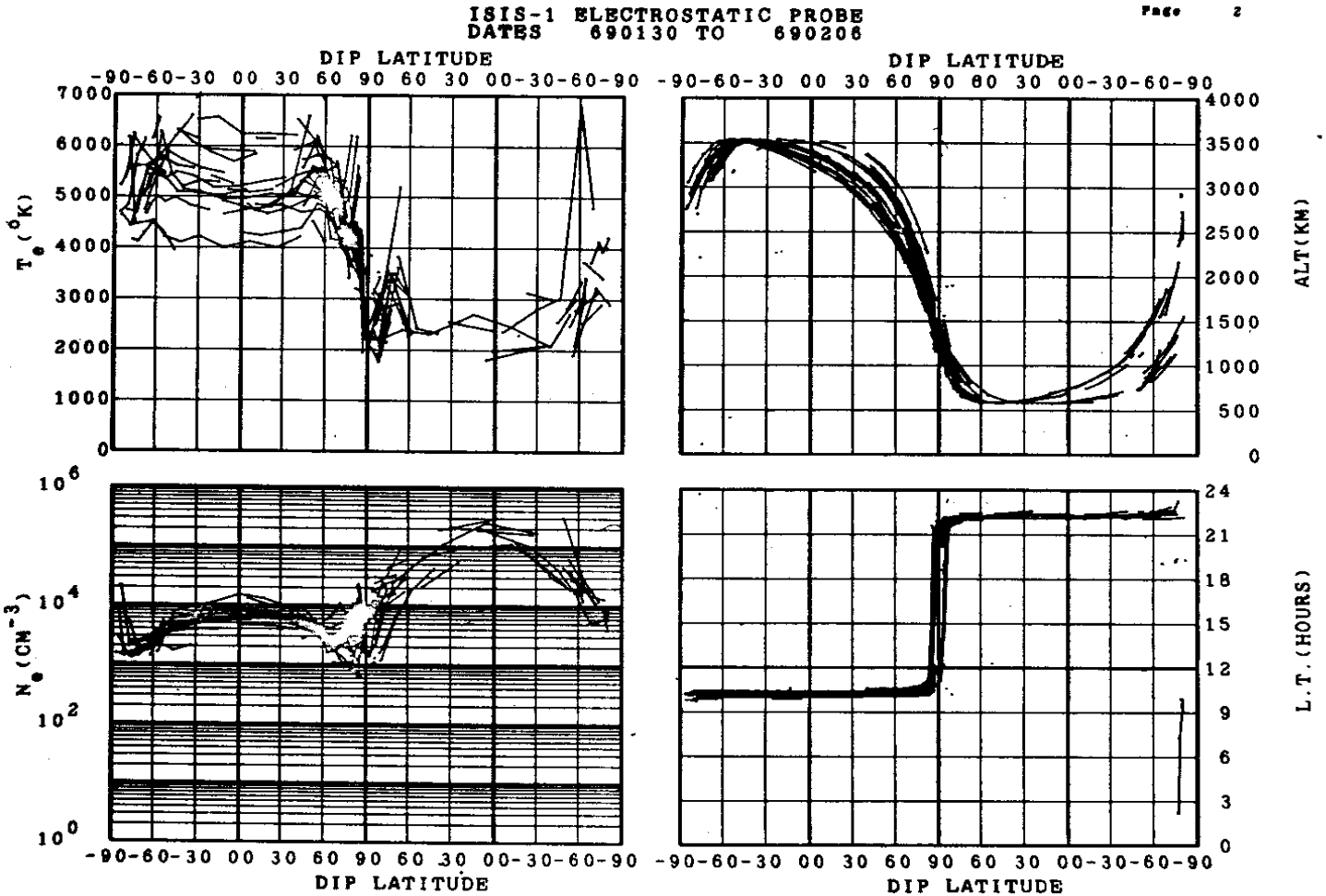

Figure 6. A typical week of ISIS-I probe measurements plotted vs dip latitude.

altitude varies symmetrically about the equator so that interhemispheric differences in the ionosphere can be seen directly. Similarly, during those periods when apogee and perigee are near the poles, the altitude varies over its entire range (600 to 3500 km) as the satellite moves from one pole to the other. At these times the altitudinal structure introduces rather large apparent assymmetries between T_e and N_e in opposing hemispheres, a fact that permits the altitudinal gradients to be evaluated. Many examples of this are evident in the plots for weeks such as this, as can be seen in many of the global plots (e.g. 67 09 06 - 13, 70 03 11 - 17, and 70 09 04 - 11) shown at the back of this report.

The Plasmapause

Although the equatorial plasmapause has received extensive study, and its correlation with troughs in the high latitude F-region has been established, there has as yet been little study of the high latitude plasmapause itself. Using the ISIS-I data, a number of questions about this part of the plasmasphere boundary are now being addressed; particularly changes in its location during magnetic sub-storms, variations with local time, and the correlation between its behavior and that found in its equatorial boundary.

When ISIS-I approaches higher latitudes on the apogee half of an orbit, the plasmapause is observed as a sharp decrease in N_e by one or two orders of magnitude. This feature is especially obvious in the winter hemisphere where the polar cap density falls to the order of 10^2/cc such as seen in the November and December data of 1969. It is interesting to note that the nightside plasmapause is also marked by a peak in T_e, a fact that perhaps reflects the heat input that is associated with the formation processes of the plasmapause itself.

The Cusp Ionosphere

In the region known as the high latitude cusp, where magnetosheath particles impinge upon the atmosphere, it is not surprising to find enhanced values of T_e and N_e. These enhancements can be seen whenever the satellite passes over the dayside auroral zone, but are particularly enhanced at higher altitudes. The period from May through June 1969 shows the cusp enhancements very clearly at about 85° dip latitude. A study of the ionosphere response to these precipitated particles is proceeding. Similar but smaller enhancements are often seen on the nightside as the satellite passes over the auroral zone.

A Dynamic View of the ISIS-I Data

The figures at the end of this report have been arranged such that a kind of motion picture of the data base can be had by performing a suitably controlled release of the pages in kinetoscope fashion. The effects of orbital precession on the local time, and of apsidal rotation on the drift of perigee, are easily

observed in this fashion. These orbital motions in turn produce readily observable changes in the T_e and N_e patterns that the satellite encounters. Shorter-term variations, such as the compression and expansion of the plasmapause during substorms, are less easily viewed in this way because they tend to occur in times shorter than one week. These effects can be observed within some of the weekly global plots such as the weeks 69 09 27 - 10 02 and 70 03 05 - 03 11.

The data shown in the global plots also exist on magnetic tape and microfilm listings that are available at the National Space Science Data Center at Goddard Space Flight Center. The data are arranged chronologically by UT and are associated with both geographic and magnetic coordinates, as well as the a_p and solar flux indices at the times of the observations.

ACKNOWLEDGEMENTS

The authors are greatly indebted to Clyde Freeman and Elbert Gregg for their efforts in processing the data and checking it for accuracy and to James Findlay for overseeing the development of the instrument and its integration into the ISIS-I spacecraft. We also express our gratitude and respect for the highly professional attitude and efforts of the Canadians at the Communications Research Center in Ottawa and at RCA Ltd, in Montreal who conceived, designed, fabricated and operated the ISIS-I satellite.

REFERENCES

Florida, C. D., "The Development of a Series of Ionospheric Satellites," IEEE, 57, No. 6, 867-875, 1969.

Whitteker, J. H., L. H. Brace, J. R. Burrows, T. R. Hartz, W. J. Heikkila, R. C. Sagalyn and D. M. Thomas, "ISIS-I Observations of the High-Latitude Ionosphere during a Geomagnetic Storm," J. Geophys. Res., 77, 6121-6128, 1972.

Brace, L. H., B. M. Reddy and H. G. Mayr, "Global Behavior of the Ionosphere at 1000 Kilometers Altitude," J. Geophys. Res., 72, 265-283, 1967.

Mayr, H. G., L. H. Brace, J. Liu, "An Empirical Temperature Model of the Ionosphere Based on Satellite Measurement Between 500 and 3500 Kilometers," EOS, 53, 473, 1972.

Brace, L. H. and N. W. Spencer, "First Electrostatic Probe Results from Explorer 17," J. Geophys. Res., 69, 4686-4689, 1964.

Brace, L. H., N. W. Spencer and A. Dalgarno, "Detailed Behavior of the Mid-latitude Ionosphere from the Explorer 17 Satellite," Planet. Space Sci., 13, 647-666, 1965.

Mott-Smith, H. M., and I. Langmuir, "The Theory of Collectors in Gaseous Discharges," Phys. Rev., 28, 727, 1926.

Spencer, N. W., L. H. Brace, G. R. Carignan, D. R. Taeusch and H. Niemann, "Electron and Molecular Nitrogen Temperature and Density in the Thermosphere," J. Geophys. Res., 70, 2665-2698, 1965.

Brace, L. H. and B. M. Reddy, "Early Electrostatic Probe Results from Explorer 22," J. Geophys. Res., 70, 5783-5792, 1965.

Brace, L. H., J. A. Findlay and G. R. Carignan, "Evaluation of Ionosphere Electron Temperature Measurements by Cylindrical Electrostatic Probes," Space Res. XI, Akademie-Verlag, Berlin, 1079-1105, 1971.

Franklin, C. A., R. J. Bibby and N. S. Hitchcock, "A Data Acquisition and Processing System for Mass Producing Topside Ionograms," IEEE, 57, 929-944, 1969.

```
IEF285I    SYS2.DUMMY                                          KEPT
IEF285I    VOL SER NOS= K3SYS2.
IEF285I    SYS2.DUMMY                                          KEPT
IEF285I    VOL SER NOS= K3SYS2.
IEF285I    SYS1.FORTLIB                                        KEPT
IEF285I    VOL SER NOS= K3SYS6.
IEF285I    SYS2.FORTLIB                                        KEPT
IEF285I    VOL SER NOS= K3SYS2.
IEF285I    SYS1.PL1LIB                                         KEPT
IEF285I    VOL SER NOS= K3SYS6.
IEF285I    SYS1.FORTSSP                                        KEPT
IEF285I    VOL SER NOS= K3SYS2.
IEF285I    SYS2.COBLIB                                         KEPT
IEF285I    VOL SER NOS= K3SYS6.
IEF285I    SYS1.ALGLIB                                         KEPT
IEF285I    VOL SER NOS= K3SYS6.
IEF285I    SYS75273.T091825.RV000.YZJRJVA1.LODMOD              PASSED
IEF285I    VOL SER NOS= K3SCR3.
IEF285I    SYS75273.T091825.SV000.YZJRJVA1.R0001120            SYSOUT
IEF285I    VOL SER NOS= K3SCR2.
IEF285I    SYS75273.T091825.SV000.YZJRJVA1.R0001121            SYSOUT
IEF285I    VOL SER NOS= K3SCR3.
IEF285I    SYS75273.T091825.RV000.YZJRJVA1.R0001122            DELETED
IEF285I    VOL SER NOS= K3SCR5.
IEF285I    SYS75273.T091825.RV000.YZJRJVA1.S0001123            SYSIN
IEF285I    VOL SER NOS= K3SCR4.
IEF285I    SYS75273.T091825.RV000.YZJRJVA1.S0001123            DELETED
IEF285I    VOL SER NOS= K3SCR4.
IEF373I STEP /LINK     / START 75273.2223
IEF374I STEP /LINK     / STOP  75273.2223 CPU    0MIN 01.89SEC MAIN 130K LCS    0K
- STEP 02 -      RETURN CODE = 0000                    STEP TIME =      .21 MINS=(CPU=      .03,IO=      .18)
                                   IO IN SECS. DISK=    10.32,DRUM=      .56,TAPE=      .00,CELL=      .00,OTHR=      .19
     XXGO        EXEC PGM=*.LINK.SYSLMOD,COND=(4,LT),REGION=70K                    00000230
     XXFT05F001 DD  DDNAME=DATA5                                                   00000240
     XXFT06F001 DD SYSOUT=&OUT,DCB=(RECFM=VBA,LRECL=137,BLKSIZE=&BLKSIZE)          00000250
     IEF653I SUBSTITUTION JCL - SYSOUT=A,DCB=(RECFM=VBA,LRECL=137,BLKSIZE=7265)
     XXFT07F001 DD SYSOUT=B,DCB=(RECFM=FB,BLKSIZE=7280,LRECL=80)                   00000260
     XXSYSPRINT DD SYSOUT=&OUT,DCB=(RECFM=VBA,LRECL=137,BLKSIZE=&BLKSIZE),         00000270
     IEF653I SUBSTITUTION JCL - SYSOUT=A,DCB=(RECFM=VBA,LRECL=137,BLKSIZE=7265),
     XX                SPACE=(CYL,(0,1)),UNIT=(DISK,3)                             00000280
     //GO.FT08F001 DD UNIT=9TRACK,DISP=(OLD,KEEP),LABEL=(01,BLP,,IN),
     //        DCB=(BLKSIZE=32000,RECFM=U,DEN=3),
     //                VOL=SER=JJ0040
     //GO.DATA5 DD *
     //
IEF236I ALLOC. FOR YZJRJVA1 GO
IEF237I 232    ALLOCATED TO PGM=*.DD
IEF237I 231    ALLOCATED TO FT05F001
IEF237I 331    ALLOCATED TO FT06F001
IEF237I 332    ALLOCATED TO FT07F001
IEF237I 331    ALLOCATED TO SYSPRINT
IEF237I 231    ALLOCATED TO SYSPRINT
IEF237I 232    ALLOCATED TO SYSPRINT
IEF237I 0C3    ALLOCATED TO FT08F001
```

RECORD 1 OF FILE 1
LENGTH = 7200 BYTES

42680000	42A40000	42511512	424FF4F7	4355F0DA	45AD70E0	443144AE	43C732DF	44380FBB	41EFD137
42503BEB	424F39C4	413415C6	42465E47	42A6AF70	44FC1278	4254D362	C06A0C40	00000000	424B07EC
424D7A52	426C3460	41DD6A60	417F9850	42680000	42A40000	425162C5	4250998A	4355EFC8	45AD70E0
44314AAE	43879191	44455EFA	41F7A16E	425076DD	424F36E4	41884856	4246A13C	42A73866	44FD2AC2
4254F18F	C02A1CA0	00000000	424B4640	424D95F9	426C5DBD	41DD6A20	41803690	42680000	42A40000
4251B1F0	4251139D	4355EEB6	45AD70E0	443150AE	00000000	4439457C	41FFD328	4250B1C1	424F3419
4111A66A	4246E7BB	42A7B59A	44FDF333	42550FAD	C014CCC0	00000000	42488475	424DB1BA	426C8203
41DD69B0	4180C200	42680000	42A40000	42520120	42519262	4355EDA4	45AD70E0	443156AE	00000000
4440EF3A	42108676	4250EC2F	424F3165	411452E5	42472E43	42A83178	44FEC00D	42552D87	C014CCC0
00000000	424BC265	424DCD90	426CA5A7	41DD6970	41814F60	42680000	42A40000	42525055	42521682
4355EC93	45AD70E0	44315CAE	43EF1ECD	443B80FB	4211163A	4251262E	424F2EC7	415FE4D7	424774D2
42A8AF1E	44FF91EB	42554B21	C05BD700	00000000	424C000C	424DE97C	426CC8A7	41DD6940	4181DEB0
42680000	42A40000	42529F8B	4252A11E	4355EB83	45AD70E0	443162AE	43DA02D1	00000000	4211ACD8
42515FBE	424F2C40	41AB4D31	4247BB62	42A92ED0	4510069D	42556879	C08D9160	41100000	424C3D65
4265FA80	424714F7	42A62970	41827030	42680000	42A40000	4252ED66	42535E54	4355EA72	45AD70E0

D-20541
DAY 104
PASS NO. 164
ALT. 1375
04/14/71 BEGINNING DAT

443168AD	43E1C8A6	00000000	42124A68	4251984F	424F29CE	4133FAB3	4247FF1E	42A98FE4	45101994
4255854A	C03F6C80	41100000	424C7A51	4265DE69	4246EFC2	42A62974	41831420	42680000	42A40000
42533D36	4253E5DF	4355E562	45AD70E0	44316EAD	43E0AF04	00000000	4212EFF1	4251D13E	424F2773
417CD158	424846F7	42AA3D17	451120E5	4255A243	C0A2E140	41100000	424C3708	4265C23D	4246D037
42A62977	4183A330	42680000	42A40000	42538CF2	4254796B	4355E852	45AD70E0	44319CAD	43C8629F
00000000	42139D77	425209BE	424F252F	4175E742	42488E99	42AABDE4	4511316A	42558EFD	C094AC00
41100000	424CF35E	4265A5F8	4246B109	42A6297E	41843630	42680000	42A40000	4253DC76	42551E88
4355E743	45AD70E0	4431A2AD	43D7F658	00000000	4214535A	425241C0	424F2300	417DF592	4248D5C9
42AB43A5	451142F7	4255DB72	C08D9160	41100000	424D2F49	426589A1	424691FE	42A62982	4184CE70
42680000	42A40000	42542B96	4255DB9D	4355E634	45AD70E0	4431A8AD	00000000	4444F7BA	42151200
42527937	424F20E8	411B87F9	42491C45	42ABCFAA	451155EB	4255F798	C01BE760	00000000	424D6AC1
424E92CC	426D8029	41DD67B0	41856D60	42680000	42A40000	42547926	42558DFD	4355E525	45AD70E0
4431AEAD	43D0FD53	4449CEB9	4215938F	4252A903	424F1EE7	41C284C6	424968DC	42AC01D2	45114C8F
42560FD8	C058D700	00000000	424DA3F0	424EAF4E	426DB87B	41DD6850	4185AD40	42680000	42A40000
4254C6B7	4256580B	4355E417	45AD70E0	443184AD	43E77156	4449F946	4216A3C1	4252DDB8	424F1CFC
41902E6C	4249ACE3	42AC8F75	451162F5	42562A8E	C08D9160	00000000	424DDE2B	424ECBE2	426DDA47
41DD67E0	41864E10	42680000	42A40000	42551359	42576FE2	4355E309	45AD70E0	4431BAAD	43E3E09B
4444DF41	42177E94	4253124D	424F1B27	4135AEDD	4249F0A9	42AD30E3	45117DBB	42564530	C06A0C40
00000000	424E1808	424EE88B	426DFB83	41DD67B0	418703D0	42680000	42A40000	42555ECB	4258E3E3
4355E1FB	45AD70E0	4431C0AD	00000000	4444DF41	42186492	425346C6	424F1968	40F7CF79	424A311E
42ADE6E7	4511A2E7	42565FC3	C0313740	00000000	424E517F	424F054A	426E1C46	41DD6770	4187CF50
42680000	42A40000	4255A8C5	425AC184	4355E0ED	45AD70E0	4431C6AD	43DBAD6E	00000000	42195631
42537B30	424F17C1	4198A46E	424A6F59	42AEB142	4511D343	42567A42	C08D9160	41100000	424E8A7E
4264DDE5	4245C363	42A6298D	4188B060	42680000	42A40000	4255F057	425C5178	4355DFE0	45AD70E0
4431CCAD	43EA5913	00000000	421A4FE2	4253AA94	424F162F	417D68A6	424AAE15	42AF5B12	4511FA13
4256523B	C0A2E140	41100000	424EC21A	4264C102	42459CE1	42A62990	41896EF0	42680000	42A40000
425636C7	425F8AC9	4355DED3	45AD70E0	4431D2AD	43CFC724	00000000	42185C64	4253E0F7	424F14B4
41377FD7	424AE745	42B0653F	45124B4F	4256ADB2	C0548C60	41100000	424EFA81	4264A40A	4245807F
42A62997	418A9370	42680000	42A40000	42567AC1	42635565	4355DDC7	45AD70E0	443200AD	43E8A31A
00000000	421C7606	42541704	424F1350	4134C4F7	424B2019	42B17C66	4513A40E	4256C8FC	C06A0C40
41100000	424F323E	426486FC	4245642F	42A6299B	418BC5A0	42680000	42A40000	4256BBD5	4267B032
4355CCBB	45AD70E0	443206AD	43DBF302	00000000	421D9CF3	42544C45	424F1202	41731CB7	424B5944
42B29A75	451412C0	4256E3DC	C0A2E140	41100000	424F6935	426469E0	424547A2	42A6299E	418CFF30
42680000	42A40000	4256F98B	426C97AB	4355DBAF	45AD70E0	44320CAD	43E45CE8	4441567A	421ED149
42548059	424F10CB	41EB1AE6	424B934E	42B3B917	45148EB0	4256FE1C	C06A0C40	00000000	424F9F4F
424FB351	426ED55D	41DD65E0	418E3950	42680000	42A40000	42574288	42730E4E	4355DAA4	45AD70E0
443212AD	4304A12F	44380E3A	421FFFE8	4254B1DA	424F0FAA	4120087C	424BDE6E	C2B2FDE2	45162B03
42571714	C0313740	00000000	424FD160	424FD095	426EA5AA	41DD65A0	418FA176	42680000	42A40000
42577AE1	42792DE6	4355D998	45AD70E0	443218AD	43DB2D50	443B80FB	42214B74	4254E02B	424F0EA0
41A86DE3	424C1EBA	C2B1F20F	4516C33D	42572E66	C06A0C40	00000000	4250051A	424FEDEA	426EBAD4
41DD6530	4190C80E	42680000	42A40000	4257ACBA	427FA6C7	4355D88E	45AD70E0	44321EAD	43DDEF5B
443E83BA	4222A64C	42550BDE	424F0DAC	41C260F2	424C5E03	C2B0FDD7	45176583	42574469	C06A0C40
00000000	42503E00	42500B51	426ED904	41DD6500	4191D595	42680000	42A40000	4257D73A	42866753
4355D784	45AD70E0	443224AD	43E0A41C	4441BDB9	424108C	42553501	424F0CCF	41F515E0	424C9B0B
C2B021CD	4519080B	4257591D	C06A0C40	00000000	42506A24	425028C7	426EFFB1	41DD64C0	4192C964
42680000	42A40000	4257F998	428D5DDA	4355D67A	45AD70E0	44322AAD	43D28D4E	00000000	42258A56
42555BC4	424F0C09	412DE935	424CD4B2	C2AF5B2B	4519B7AD	42576C9B	C054BC60	41100000	42509B4D
4263B9AE	4244D210	42A629B8	4193A656	42680000	42A40000	42581D0D	42952506	4355D570	45AD70E0
443230AD	43D48BB2	00000000	422706D2	425579DB	424F0B59	418B89FC	424D159F	C2AEA756	4518B738
42577BC0	C0B11680	41100000	4250C9F1	42639C11	4244C1A0	42A629BB	41946FFE	42680000	42A40000
425827EA	429BF49D	4355D467	45AD70E0	443236AD	43DA7E19	00000000	4228A54D	4255A25E	424F0AC0
4181F0AC	424D4C7A	C2ADF90F	451C20C2	4257901B	C094AC00	41100000	4250F9C8	42637E66	424474D8
42A629BF	41963228	42680000	42A40000	42582858	42A289F8	4355D35E	45AD70E0	443264AD	43D96804
00000000	422A528B	4255CF41	424F0A3D	413A2AC7	424D66EE	C2AD413B	451DC432	4257A6AC	C054BC60
41100000	42512862	426360A9	42442712	42A629C6	4195FE0C	42680000	42A40000	42581E51	42A9691E
4355D256	45AD70E0	44326AAD	43CF5070	00000000	422C0D2B	425605DA	424F09D1	41312A07	424D8A71
C2AC76DF	451E6C56	4257C21C	C054BC60	41100000	4251559A	426342D9	4243DCF9	42A629C9	4196DD3F
42680000	42A40000	425809F1	42AFF68C	4355D14E	45AD70E0	443270AD	43D9A811	4445C639	422DD387
42564CA2	424F057C	41457098	424DACCD	C2AB92EA	452009FF	4257E5A8	C06A0C40	00000000	4251814F
4250DB04	427063E7	41DD6330	4197D759	42680000	42A40000	4257DB54	C2B12AA3	4355D046	45AD70E0
443276AD	43D7C9F6	4448D2F9	422FB66F	42570288	424F093D	41C6ABF5	424DCCCF	C2AA4294	4520B76D
42584103	C06A0C40	00000000	4251AD0A	4250F8F3	4270800E	41DD62F0	41994389	42680000	42A40000
4257AFFD	C2AAE8EA	4355CF3F	45AD70E0	44327CAD	00000000	4447633A	423191D8	425792DE	424F0915
40F343BD	424DF3FD	C2A90D95	45224E27	4258893E	BFDB2200	00000000	4251D59E	425116F1	4270B496
41DD62C0	419A934C	42680000	42A40000	42577D02	C2A4F522	4355CE38	45AD70E0	443282AD	43D30839
444A9D39	42337C8E	42582E95	424F0903	41319DDB	424E1FCA	C2A7BFE5	4522E3D0	4258D73B	C0468720
00000000	4251FC3B	42513500	4270910F	41DD6250	419BFD61	42680000	42A40000	42574345	C29F5AE0
4355CD32	45AD70E0	443288AD	43D1FA32	445059CC	42354F8F	42588437	424F0908	419DBEEE	424E509C
C2A65CE7	45236F3A	42591A1C	C07126E0	00000000	425220C7	4251531E	42704741	41DD6210	419D7E20
42680000	42A40000	42570384	C29A24C4	4355CC2C	45AD70E0	44328EAD	43C849F7	00000000	42372B99
4258D761	424F0924	41879A6B	424E8634	C2A4E85E	4524EC46	42592BB3	C0A2E140	41100000	4252433E
42628EB6	424A2283	42A629E3	419F11AD	42680000	42A40000	4256B4A2	C2950882	4355CB27	45AD70E0
443294AD	43C7D37B	00000000	42390DD2	4257F056	424F0956	412B7517	424EC37B	C2A32D15	45256DCD
4258B811	C05BD700	41100000	4252646A	4262707B	4244E031	42A629E6	41A0F001	42680000	42A40000
425671A9	C290DE6B	4355CA22	45AD70E0	44329AAD	43CEFC0B	00000000	423AD3BF	42575BFA	424F099F
417D4454	424EFE43	C2A1B896	4525D4A5	42586DBE	C094AC00	41100000	42528229	4262522F	42454E44
42A629ED	41A28058	42680000	42A40000	42562C12	C28D3217	4355C91E	45AD70E0	4432C8AD	43C788CD
00000000	423C8C05	4256CCC4	424F09FF	41B77CEE	424F38DC	C2A042C8	45272B9E	425825F0	C0A2E140
41100000	42529DBF	426233D4	4245ABEA	42A629ED	41A4182C	42680000	42A40000	4255E455	C28A046E
4355C81A	45AD70E0	4432CEAD	43D59C83	00000000	423E3384	425658ED	424F0A75	41328C6A	424F71A0

00000000	42456CD9	424B6F7B	42686BE3	41D29F30	41803150	42680000	42A50000	424918A8	422E69C8
4356 0B6A	45AD70E0	447BE8B7	43DED6BF	443E83BA	4184CC00	42475301	424F9EDF	41F5807A	4241D1E9
428C9089	44F31532	425022DA	C062F1A0	00000000	4245B07C	424B8868	426896D1	41D29FD0	4180A500
42680000	42A50000	42496995	422E82D2	43560A50	45AD70E0	447BEEB7	43E4B7D8	443FB97B	41882873
42479FE6	424F99B5	41528885	42421780	428CF6AC	44F332AB	42504CA2	C07126E0	00000000	4245F3DA
4248A16F	4268C15B	41D29E80	41811AB0	42680000	42A50000	4249BA7C	422E9D01	43560936	45AD70E0
447BF4B7	00000000	4440208B	418BA4D5	4247ECAA	424F94A1	41124DAB	42425D2A	428D5F25	44F37937
4250763D	C0230200	00000000	42463706	424BBA92	4268EBBD	41D29F30	41819300	42680000	42A50000
424A0B5E	422EB869	4356081C	45AD70E0	447BFAB7	00000000	443EEAFA	418F4294	42483956	424F8FA2
4110A0DA	4242A255	428DCA05	44F3C0EA	42509FAD	C014CCC0	00000000	424679FD	424BD3CE	426915F8
41D29EF0	41820DE0	42680000	42A50000	424A5C3C	422ED51C	43560704	45AD70E0	447C00B7	43E3F269
00000000	4193032A	424885DD	424F8AB9	416C7C82	4242E72D	428E3760	44F3E1D2	4250C8F1	C0A9FBE0
41100000	42468BBD	426812D9	424ABFF8	42A0614	41828B70	42680000	42A50000	424AAD11	422EF38D
435605EB	45AD70E0	447C06B7	43D9857E	00000000	4196E8C9	4248D248	424F85E4	41952AC0	42432BA3
428EA77F	44F42C5B	4250F20A	C0B11680	41100000	4246FF4D	4267F968	424A95F2	42A6D618	41830C00
4268C000	42A50000	424AFDE4	422F12E0	435604D3	45AD70E0	447C0CB7	43E0FF68	00000000	419AF35A
42491E9A	424F8126	41222E8B	42436FD4	428F19EA	44F44FBA	42511AFB	C062F1A0	41100000	4247418E
4267DFDD	424A6C4A	42A6D61F	41838F10	42680000	42A50000	424B4EAF	422F33C4	435603BC	45AD70E0
447C3AB7	43D48B1D	00000000	419F2592	42496AC8	424F7C7C	41568A6C	4243B3A9	428F8F0E	44F49C90
425143C1	C09BC6A0	41100000	4247838F	4267C635	424A42C9	42A6D623	41841500	42680000	42A50000
424B9F74	422F545B	435602A5	45AD70E0	447C40B7	44106886	00000000	41A38135	4249B6D6	424F77E9
4131235E	4243F71E	42900704	44F4C2FE	42516C5E	C0DBB630	41100000	4247C54E	4267AC78	424A1970
42A6D626	41849E00	42680000	42A50000	424BF031	422F7AC8	4356018F	45AD70E0	447C46B7	43DB4A40
443CE6BA	41A8081A	424A02C4	424F736A	414CC0F3	42443A2E	429081E8	44F51327	425194D1	C062F1A0
00000000	424806C6	424C6D62	426A0FC9	41D29D60	41852A30	42680000	42A50000	424C40D9	422FA43A
43560079	45AD70E0	447C4CB7	00000000	4449677A	41ACB6C2	424A4E7F	424F6F02	41174B07	42447C72
42910178	44F567FF	4251BD12	C014CCC0	00000000	424847AB	424C8754	426A39AE	41D29D20	4185BB70
42680000	42A50000	424C9183	422FCD47	4355FF63	45AD70E0	447C52B7	43E56001	443C7F7A	41B19920
424A9A25	424F6AAF	41A0605B	4244BE9C	429182BF	44F58C7B	4251E531	C062F1A0	00000000	42488885
424CA15D	426A62C0	41D29CF0	41864E80	42680000	42A50000	424CE224	422FF860	4355FE4E	45AD70E0
447C58B7	43E6774A	44428C3B	4186AD2E	424AE5A1	424F6671	4141A91A	4245005D	4292071A	44F5EAE3
4252CD26	C062F1A0	00000000	4248C914	424CBB81	426A8B9C	41D29C80	4186E4E0	42680000	42A50000
424D328D	423025AD	4355FD39	45AD70E0	447C5EB7	43E80B9A	443CE68A	41BBF516	424B30FB	424F624A
417B30EB	424541B0	42928EA1	44F6435C	425234F2	C06A0C40	00000000	42490955	424CD5BC	426AB446
41D29C80	41877EB0	42680000	42A50000	424D834C	4230555B	4355FC25	45AD70E0	447C64B7	43F1811E
00000000	41C1730D	424B7C32	424F5E38	41314669	42458292	42931970	44F69E0F	42525C95	C03F6C80
41100000	42494942	42670FF1	42492342	42A6D63F	41881C10	42680000	42A50000	424DD3C9	42308925
4355FB11	45AD70E0	447C6AB7	43EE7F5B	00000000	41C72691	424BC737	424F5A3C	41A674D9	4245C2CE
4293A867	44F6FC9D	4252840A	C0B11680	41100000	42498888	4266F584	424BFA9C	42A6D643	4188BDE0
4268C000	42A50000	424E2446	4230BD45	4355F9FE	45AD70E0	447C70B7	43F1C79C	00000000	41CD1921
424C1220	424F5656	41B41897	424602DB	4294399D	44F75B7B	4252AB5E	C0B11680	41100000	4249C800
4266DAFF	4248D2C2	42A6D647	41896220	42680000	42A50000	424E74B6	4230F477	4355F8EB	45AD70E0
447C9EB7	43DE489D	00000000	41D34899	424C5CE4	424F5286	41221BE0	42464264	4294CE77	44F7BD3A
4252D288	C04DA1C0	41100000	424A06E1	4266C064	4248AB16	42A6D64E	418A0A40	42680000	42A50000
4246C517	42312F1F	4355F708	45AD70E0	447CA4B7	43E2C37F	00000000	41093722	424CA776	424F4ECB
412C6C35	42468163	42956722	44F82238	4252F986	C062F1A0	41100000	424A4552	4266A5B0	42488392
42A6D651	418AB680	42680000	42A50000	424F1569	42316DAE	4355F6C6	45AD70E0	447CAAB7	43E5E4AE
4438DE3A	41E066E7	424CF1D7	424F4B27	41A1B1F0	42468FCC	429603C9	44F88ADE	42532058	C062F1A0
00000000	424A834C	424D751A	4268A3D6	41D29AB0	418B6710	42680000	42A50000	424F6545	4231C51A
4355F5B4	45AD70E0	447CB0B7	43E8263C	4440EF3A	41E737DE	424D3B6B	424F4798	41A1F564	4246FB47
4296ADD2	44F90AD4	425346B0	C06A0C40	00000000	424ABF9D	424D8FFD	426BCE3C	41D29A70	418C25D0
42680000	42A50000	424FB562	42321003	4355F4A2	45AD70E0	447CB6B7	00000000	443CE6BA	41EE6B85
424D853F	424F4420	41B65A6	4247381D	4297541C	44F9A70E	4253 6D17	C014CCC0	00000000	424AFC72
424DAAF1	426BF5D9	41D29A40	418CE0A0	42680000	42A50000	42500574	42325E64	4355F391	45AD70E0
447C8CB8	43F361A5	4441567A	41F5EAA8	424DCEE9	424F40BE	41343BE0	42477480	4297FE01	44FA1E8A
42539355	C04DA1C0	00000000	424B38D7	424DC602	426C1D21	41D29A00	418D9F60	42680000	42A50000
42505575	4232B090	4355F280	45AD70E0	447CC2B8	43FF4FA7	4439ACBB	41FDB748	424E1855	424F3D71
41607788	42478064	4298AB8E	44FA9992	4253B966	C06A0C40	00000000	424B74BE	424DE129	426C4408
41D29990	418E6200	42680000	42A50000	4250A565	42330707	4355F170	45AD70E0	447CC8B8	441071F7
00000000	42105C43	424E6190	424F3A3B	414C20A9	4247EBC6	42995CF3	44FB40A4	4253DF4A	C0C66660
41100000	424BB022	42660398	42479568	42A6D66A	418F28D0	42680000	42A50000	4250F50F	42336CE1
4355F060	45AD70E0	447CCEB8	43F9F2D9	00000000	4210E323	424EAA38	424F371B	412A5505	42482588
429A1680	44FBF620	425404D6	C04DA1C0	41100000	424BEA80	4265E84D	42476DCA	42A6D66E	418FF830

RECORD 2002 OF FILE 1
LENGTH = 7200 BYTES

DAY 151 PASS NO. 769 ALT. 1423

42970000	43301000	42334E71	C255ACF2	4358FF2E	45AD7830	452FB0D2	43E22A76	00000000	415D8940
424234C7	42270A7A	419D4DDB	423E250F	C2150E00	45228008	424D482F	3F79DC00	41100000	424191C6
428A3A11	424C86FD	428240E7	41E13B4A	42970000	43301000	42334E71	C255ACF2	4358FF2E	45AD7830
452FB0D2	43E4EEEB	00000000	415D8940	424234BC	42270A7A	41A58830	423E250F	C2150E00	45228008
424D482A	3F79DC00	41100000	424191C6	4298AE02	4251D413	42781604	41E13B4A	42970000	43301000
4232FDF0	C255ACD1	4359001E	45AD7830	452FB132	4410B722	00000000	415BA390	4241E0B9	4226DEB9
4115380E	423DD514	C214FA75	4522813A	424D17F4	3F79DC00	41100000	4241 4D14	4298B82E	42515F77
42781604	41E158F0	42970000	43301000	4232FDF0	C255ACD1	4359001E	45AD7830	452FB132	4410E605

D- 20541
DAY 151
PASS NO. 769
ALT. 1423
05/31/71 END DATE